Synthesis of NiO nanoparticles prepared via a green process using Azadirachta indica, Morinda citrifolia, and Terminalia elliptica for biological applications

Lakshmikanth Reddy V (lakshmikanthreddypdtr@gmail.com)
Lakshmikanth S

Research Article

Keywords: Green synthesis, NiO NPs, Antibacterial activity, Antioxidant, Characterization techniques

Posted Date: September 28th, 2022

DOI: https://doi.org/10.21203/rs.3.rs-2069010/v1

Additional Declarations: No competing interests reported.

Version of Record: A version of this preprint was published at BioNanoScience on June 29th, 2023. See the published version at https://doi.org/10.1007/s12668-023-01145-7.

Abstract

Developing a low cost, high-efficiency and environmentally friendly approach to synthesize nickel oxide (NiO) nanoparticles (NPs) for biomedical applications has become a research focus in the current scenario. In the present investigation, the NiO NPs were synthesised via a green process using different plant extracts, such as *Azadirachta indica* (N1), *Morinda citrifolia* (N2), and *Terminalia elliptica* (N3). X-ray diffraction (XRD), Field emission scanning electron microscopy (FESEM), Energy dispersive x-ray analysis (EDX), X-ray photoelectron spectroscopy (XPS), and photoluminescence excitation spectroscopy were used to investigate the evolution of the size, morphology, chemical composition, and surface defect of NiO NPs. The synthesized NiO NPs were exhibited as cubic structures. As compared to conventional antibiotics amoxicillin, *Morinda citrifolia* (N2) and *Terminalia elliptica* (N3) medicated NiO nanoparticles, *Azadirachta indica* mediated NiO (N1) exhibits more antibacterial activity. From the antioxidant activity, the DPPH assay of N1, N2, N3, and vitamin-c samples exhibited free radical scavenging potential. There are increases in the inhibition percentage with increases in the concentrations of these NiO NPs. In addition, the N1 sample demonstrates higher radical scavenging activity than N2 and N3. From the observed results, we believe that *Azadirachta indica* mediated N1 condition synthesized NiO NPs are very promising biocidal nanomaterials against human pathogens, which will be medically crucial for clinical applications.

Introduction

The emergence of drug-resistant bacteria remains a critical public-health challenge because it is associated with high mortality, morbidity, and treatment costs [1]. Researchers have made efforts to develop alternative therapeutic approaches in the face of increasing resistance to frontline antimicrobial agents and an increase in infections caused primarily by multidrug-resistant organisms. Because of the unique properties of nanomaterials, the application of nanotechnology appears to be a viable solution. According to their semiconducting nature and sizeable active surface area, metal oxide nanoparticles such as ZnO [2], CuO [3], SnO_2 [4], TiO_2 [5], and CeO_2 [6] nanoparticles are good choices for biomedical application. However, despite the wide usage of different semiconductor metal oxide nanomaterials as biocidal materials [7]. Amongst NiO, the most essential wide bandgap p-type metal oxide semiconductor that can be used in various applications [8–11]. The crystallinity, phase composition, size, and morphology of NiO enhance its performance in many applications [12, 13]. The Size, shape and surface area of materials, especially in biocidal applications, has a vital role in improving bacterial killing efficacy [14]. In recent decades, various synthesis techniques have been followed for preparation of nanoparticles, such as sol-gel, hydrothermal, precipitation techniques, emulsions, and the green method [15]. However, among different methods, the synthesis of NiO nanostructured materials using the green process approach (using plant extract) has attracted the broadest attention because of its simple, cost-effective, eco-friendly, biocompatible one and scalable production. The biomolecules functionalized plant extract acts as a reducing and a capping agent. Nanoparticles are made less and more stable by phytochemicals in the plant extract. These phytochemicals include alkaloids and amino acids, ascorbic acid and a

carboxylic acid, polyphenols, flavonoids, alcohols and terpenes, glycosides, carbohydrates, thiamin, vitamin C, and polyphenol components [16, 17]. Size distribution, shape, surface charge, surface chemistry, capping agents, and other variables all influence the biological activity of inorganic NPs. However, when it comes to the synthesis of NPs, the capping agent is among the essential elements. As a result, selecting appropriate capping moieties is critical for stabilizing colloidal solutions and their incorporation into various plant extract and the environment.

In the present work, from different leaves extracts, *Azadirachta indica* (N1), *Morinda citrifolia* (N2), and *Terminalia elliptica* (N3) were used to prepare the NiO NPs. In characteristics of *Azadirachta indica* has a complex of compounds, including nimbin, nimbidin, nimbolide, and limonoids, which play a role in patient care by modulating multiple genetic pathways other activities. However, the *Morinda citrifolia* contains fatty acid glycosides, iridoids, anthraquinones, coumarins, flavonoids, lignans, phytosterols, carotenoids, and various volatile compounds such as monoterpenes, short-chain fatty acids, and fatty acid esters; it will cure different diseases (antibacterial, antiviral, antifungal, antitumor, anthelminthic, analgesic, hypotensive). Among them, Tannins, flavonoids, phenolic acids, triterpenes, triterpenoids glycosides, lignan, and lignan derivatives are among the phyto-compounds in the Terminalia elliptica plate, which is used for a broad spectrum of biological activities. The NiO NPs were successfully synthesized through a green process using different plant extracts like *Azadirachta indica, Morinda citrifolia, and Terminalia elliptica* as capping agents. The resulting nanomaterials were characterized further to study their optical, structural, and biocidal properties.

Experimental Procedure

2.1 Materials

Nickel (II) nitrate hexahydrate (≥98.5%: CAS Number 13478-00-7), Neodymium (III) nitrate hexahydrate (99.9%: CAS Number: 16454-60-7) have been purchased from Sigma Aldrich.

2.2 Plant extract preparation

The freshly collected *Azadirachta indica, Morinda citrifolia*, and *Terminalia elliptica* leaves were washed several times with de-ionized water to remove the adhering foreign impurities. The *Azadirachta indica, Morinda citrifolia*, and *Terminalia elliptica* leaves extract were developed by taking 10 gms of fresh leaf boiled at a temperature of 80 ˚C in 100 mL of de-ionized water for 15 mins. Followed by, leaves extract were filtered using filter paper.

2.3 Preparation of NiO NPs

To synthesize NiO NPs, the 0.1 M of Ni $(NO_3)_2$.$6H_2O$ salt was dissolved into the different plant extract solution (*Azadirachta indica, Morinda citrifolia*, and *Terminalia elliptica*). The plant extract metal Ni^{2+} ions solution was heated at 80˚C for 6 hrs using a reflux condenser to avoid solvent evaporation. After 5 hrs, both the solutions were brought back to room temperature and evaporated at 120˚C to remove the

moisture and annealed at 800˚C for 5 hrs. Synthesis of NiO NPs prepared via diffract plant extract such as *Azadirachta indica, Morinda citrifolia*, and *Terminalia elliptica* as shown in scheme 1.

2.4 Antibacterial assay

Determination of antibacterial activity was done well diffusion process against the test *S. aureus, B. megaerium, K. pneumonia* and *S. dysenteriae* bacterial strain on Nutrient agar, according to the Clinical and Laboratory Standards Institute (CLSI) [18].

2.5 Characterization techniques

The NiO NPs were subjected to different characterization techniques: X-ray diffraction pattern using X'PERT PRO PAN analytical, measured in the range between 20^o - 80^o at source CuKα (1.54 Å) was used. The oxidation state and surface functionalization of the materials were identified by XPS measurement. The topography and elemental composition were observed from FESEM with EDAX (Carl Zeiss Ultra 55FESEM and Inca: EDX). The functional group analysis was studied using FTIR spectrum recorded in the range 4000-400 cm^{-1}. The PL measurement was carried out by using a Cary Eclipse spectrometer.

Results And Discussion

3.1 Surface morphology and particle size of the NiO nanoparticles

The biocidal properties of the material are greatly governed by their external morphologies and size. The low dimensional particles improve the biocidal performance of the materials because of their large surface to volume ratio and better carrier transition. Generally, diverse morphologies can have the ability to tune the chemical activity, and biocidal properties [19].

The surface morphology of the obtained ultrafine NiO nanomaterials was evaluated using field emission scanning electron microscope (FESEM) and presented in Fig. 2a-c. The average grain size (~ 150–500 nm) was obtained using *IMAGE J* software (Fig. 2a-c). The NiO NPs extracted from the *Azadirachta indica* leaves were observed to be large grains with different facets at the bottom part and small crystallites aggregates on the surface of these large crystallites, which were very vivid in the electron micrograph (Fig. 2a). On the other hand the NiO nanocrystals synthesized from *Morinda citrifolia*, and *Terminalia elliptica* leaves solution were found to be spherical in shapes with fairly uniform distribution (Fig. 1b-c), due to the proper reaction of Ni solution in the reflux condenser at 80 ºC for 4 hrs followed by slow cooling. Also, the crystallites size was detected to be less (Fig. 2b-c) as compared to the NiO NPs extracted from the *Azadirachta indica* leaves (Fig. 1a). The determination of particle size from the SEM images were more accurate estimation hence, the particle size was further evaluated by measuring the changes in the intensity of light scattered from a nickel oxide suspension. From the dynamic light scattering (DLS), the particle diameter was observed to be varied from 50 to 1000 nm, but the high

diffraction intensity was noticed near to 150–300 nm in all the plots, depicted in the supplementary information (S1a-c). The NiO NPs extracted from the *Azadirachta indica* leaves exhibits higher diameter ~ 500 nm, the results is in accordance with the FESEM.

The SEM images (Fig. 1b-c) shows spherical shaped structure of NiO, but the NPs synthesized from the *Azadirachta indica* leaves possess faceted microstructures with non-uniform distribution (Fig. 2a). In order to explain the top-down growth mechanism of the nanocrystals, the growth mechanism explained through schematic diagram (Fig. 3) resemblance to the FESEM images (Fig. 2a-c) similar to Ekernoth et al. [3]. From the schematic (Fig. 2a) it's very clear that the cavities originated in between the faceted NiO particles are due to the improper merging of the different grains, which are analogues to the electron micrographs (Fig. 2a). But the NiO NPs synthesized from the leaves were found to uniform particle distribution with less cavities. Also, the particle size was estimated to be small as compared to the nickel oxide extracted from Ni (supplementary information S1a-c), this is mainly due the reaction process of the N1, N2 and N3 leaves.

3.2 X-ray diffraction studies

In general, X-ray diffractometer is a figure print technique to elucidate the monophase nature of the synthesized materials. Thus, the structural characterization of the NiO nanoparticles was investigated using power X-ray diffractometer (PXRD of model: XPERT-PRO). The X-ray diffractograms of the nanoparticles extracted by green synthesis method are presented in Fig. 3. All the diffraction profiles recorded from 10 to 80° with a scan rate of 0.02° and step size at 0.050º. The PXRD peaks were indexed for the low dimensional NiO samples grown at different level of oxygen and were compared with the standard JCPDS data base (Card No: 47-1049).

PXRD spectra confirmed the cubic crystal structure with face centered cubic (FCC) phase of NiO as shown in Fig. 4(a-d). The five prominent diffraction peaks (111), (200), (220), (311) and (222) emerged at 2θ angles of 37.33°, 43.38°, 62.84°, 75.36°, and 79.22°, respectively. A highly intense diffraction peak was observed at an angle 2θ of 43.38° which corresponds to the plane (200) orientation of cubic NiO lattice. The absence of other peaks, justifies that the synthesized NiO nanoparticles possess cubic crystal structure with FCC phase. The particle size was estimated using the Debye–Scherrer equation, crystallite size (D) = $\frac{0.9\lambda}{\beta\cos\theta}$, where λ represents the wavelength of light (K_α = 1.54056 Å), β is the full-width at half maximum (FWHM) is equal to 0.1968 Å of peak (200) and θ is the Bragg's angle to surface of the plane. The calculated crystallite sizes of the NiO is 96.95 nm, which is in accordance with the average particle size estimated from the SEM images. The lattice parameter (a) of the synthesized products were calculated as 4.766 Å using the standard formula (1),

$$a^2 = \frac{\lambda^2(h^2 + k^2 + l^2)}{\sqrt{\left(4sin^2\theta\right)}}$$

1

where λ is the wavelength of x-rays, *h*, *k* and *l* are the Miller indices and *a* is the lattice parameter also the dislocation density, $\delta = 1/D^2$ were calculated using this formula and tabulated in the Table 1.

Table 1
Crystallographic parameters of the NiO nanoparticles

Peak Positions (degree)	Peak Heights (Counts/second)	Planes	FWHM	Crystallite size (nm)	Dislocation density $\times 10^{-3}$ (1/nm)
37.36	1540.89	(111)	0.1476	118.18	8.462
43.39	2893.42	(200)	0.1968	96.95	10.315
62.94	1334.77	(220)	0.1968	154.87	6.457
75.48	498.21	(311)	0.1476	374.67	2.669
79.46	310.68	(222)	0.1476	513.53	1.947

3.3 Energy dispersive X-ray analysis

The elemental in-homogenity is significantly controlled by the performance of the crystals, because the presence of impurities may enhance or decrease physical properties of the material. Hence, to probe the quality and elemental composition of the NiO nanoparticles the energy dispersive X-ray analysis (EDX) was employed. Figure 5(a-c) shows the EDS spectra of the nickel oxide NPs extracted from the green synthesis method. From the Fig. 5a, it was very clear that the elemental percentage of the nickel in the NiO NPs were observed to be less, which was grown from the *Azadirachta indica* leaves. This result suggests that, there has a slight compositional variation in the elemental nickel and the oxygen, due to the improper development of the growth. The big cavities have been noticed in SEM (Fig. 2a) of these NPs, this may be emerged due to the Ni vacancy in the crystal. On the other hand the low dimensional NiO particles synthesized from the *Morinda citrifolia*, and *Terminalia elliptica* leaves exhibits homogeneous proportion of elements (.at %). This result clearly indicates that the NPs do not contain any multiphase other than nickel and oxygen. Hence the nanoparticles synthesized by the green method can be effectively utilized for the biomedical application.

3.4 X-ray photoelectron spectroscopic analysis

The valence electronic states of the synthesized samples were further characterized by X-ray photoelectron spectroscopy (XPS). In the present work, all the XPS spectra were presented the binding energy (BE) values decreasing from left to right. The wide-scan NiO XPS spectrum in Fig. 6a, justifies that the presence of only nickel, oxygen and carbon elements in the sample. All the peaks were identified and indexed in the Fig. 6a-c, which were calibrated using the carbon (C1s) peak positioned at 284.6 eV. The peak emerged at 284.6 eV and 288.19 eV in the core-level spectrum of C1s is due to the strong binding of C – C and C = O, respectively [20]. The Ni 2p spectra were split based on the spin–orbit coupling, Ni $2p_{1/2}$ and Ni $2p_{3/2}$ peaks analogous to the binding energy in the range of 850 to 869 eV and 870 to 885 eV,

respectively [21]. Figure 5c represents the core-level spectra of the Ni 2p, were all the peaks were indexed as per the standard literature [21]. The satellite peak Ni $2p_{1/2}$ (NiO) positioned at 879.57 eV, the BE as 875.05 eV and 871.80 eV is owing to the multiplet-split at Ni $2p_{1/2}$. The satellite peak at 862.93 eV representing the Ni $2p_{3/2}$ (NiO) and Ni $2p_{3/2}$ was originated due to the multiple-split at 857.61 eV. The component at 529.91 eV corresponds to double bonded oxygen in the carboxylic group (O = C – OH) when the other component at 533.25 eV was may be attributed to an oxygen atom in C – OH bond (O = C – OH) [22]. Even though the peaks emerged only from the NiO nanoparticles, but the slight shift in the BE is corresponding to the higher oxidation states. Also, the shift with noise peak was related to the satellite peak or shake up and it is a case for only some metal or its oxide.

3.5 FTIR spectroscopic analysis

The functional groups present in the NiO nanocrystals extracted from three different leaves (N1, N2 and N3) using the green synthesis method, were analyzed by Fourier transform infrared spectroscopy (FTIR) at room temperature in the spectral range of 400 to 4000 cm^{-1}. Figure 7 shows the FITIR spectra of the nickel oxide particles, which showed several significant absorption peaks. The strong absorption band at 600–700 cm^{-1} in the NPs extracted from N1 and N3 is assigned to Ni—O stretching vibration mode, but such peaks were absent in the nanoparticles extracted from N2. The broad absorption band centered at 1635 cm^{-1} is attributed to the H—O—H bending vibrations mode, this is also due to the adsorption of water in air during the pellet preparation or the presence of H_2O content in the sample during the synthesis process. The broad band originated at 3400–3500 cm^{-1} corresponding to the stretching vibration mode of the chemically bonded O-H hydroxyl group which is generally connected with the water [23]. This is prominent in the NPs extracted from the *Azadirachta indica* and *Morinda citrifolia* than Terminalia elliptica leaves. These observations provided more evidence to the presence of hydration in the synthesized structure. Meanwhile, it implied the presence of hydroxyl in the precursor, and the broad absorption around 767 cm^{-1} is assigned to the band C = O stretching vibrations. The sharp bands were observed at 1600 to 1500 cm^{-1} related to the = CH stretching and —C = H bending vibrations which may indicate the presence of aldehyde groups, amides groups, and carboxylic acids [24]. It is worth to note that, the peaks around 1750 – 1060 cm^{-1} corresponding to the presence of ethers, i.e., 1159 cm^{-1} show the C—O stretching vibrations. The weak absorption peak observed at 1000–1500 cm^{-1} are assigned to the O—C = O and C—O symmetric as well as asymmetric stretching vibrations, respectively. But in the present work, the NPs extracted from the N3 leaves exhibits a very small intensity of absorption peaks at 1000–1500 cm^{-1}, which indicates that the ultra-fine powders have a strong physical absorption to H_2O and CO_2.

3.6 Photoluminescence spectrum

The photoluminescence spectrum of green synthesized NiO NPs is shown in Fig. 8, and the exciting wavelength is at 325 nm. The PL emission spectra of values observed at (368, 392, 416, 441, 457, 481,

and 545 nm) for the N1 sample, (370, 391, 402, 440, 481, and 523 nm) for the N2 sample, and (363, 390, 420, 457, 468, and 484 nm) for the N3 sample, respectively. The UV emission peaks were found to be (368 and 392 nm), (370 and 391 nm), and (363 and 390 nm) for N1, N2, and N3 samples, respectively. The violet emission peak, located at 402 nm for the N2 sample, is owing to the energy transition of trapped electrons at the Ni interstitial to the VB. The strong blue emission was located at (416, 441, 457, and 481 nm), (440 and 481 nm), and (420, 457, 468, and 484 nm) for N1, N2, and N3 samples, respectively. In this case, electrons from the double ions Ni vacancy (V^{2-}_{Ni}) radiatively combine with holes in the VB. The green emissions were centered at 545 nm and 523 nm for the N1 and N2 samples, respectively, which correspond to defects caused by charge transfer between Ni^{2+} and Ni^{3+} in the NiO lattice interstitial oxygen trapping and Ni vacancies [7].

3.7 Antibacterial properties

The potential antibacterial activity of the N1, N2, and N3 nanomaterials was performed against *S. aureus, B. megaerium, K. pneumonia* and *S. dysenteriae* bacteria and was carried out by using the well diffusion method. The results are shown in Fig. 9. and zone of inhibition values are given in Table 2. The N1, N2, and N3 nanomaterials and the conventional antibiotic amoxicillin exhibit antibacterial activity. The N1 sample exhibits the highest antibacterial activity compared to the N2 and N3 conventional antibiotics, Amoxicillin. Metal oxide nanoparticles kill bacteria by making active free radicals called reactive oxygen species (ROS), releasing metal ions called Ni^{2+} ions, and having surface flaws called oxygen vacancies. The photoluminescence study shows oxygen vacancies are higher in the N1 nanomaterials when compared to N2 and N3 NPs. The green emission at 545 and 523 nm for N1 and N2 samples. The increasing green emission band value shows an enhancement of oxygen vacancies, which is attributed to the N1 sample that can be able to produce more ROS. These ROS can damage bacterial cell components, such as nucleic acid, proteins, and macromolecules (DNA, lipids, and carbohydrates). For example, the active free radicals hydrogen peroxide and hydroxyl radical penetrate the bacterial cell, which causes undesired reactions and affects the cell's biological process, significantly affecting cell growth and leading to cell death [25].

Table 2
Zone of inhibition of NiO nanomaterials tested against *S. aureus*, *B. megaerium*, *K. pneumonia* and *S. dysenteriae* bacterias

Bacterial name	N1 (A) (mm)	N2 (M) (mm)	N3 (N) (mm)	Amoxicillin (mm)
S. aureus	20 ± 1	13 ± 0.65	15 ± 0.75	25 ± 1.25
B. megaterium	19 ± 0.95	15 ± 0.75	16 ± 0.8	19 ± 0.95
K. pneumonia	21.5 ± 1.075	11 ± 0.55	16 ± 0.8	22 ± 1.1
S. dysenteriae	21 ± 1.05	14.5 ± 0.725	15 ± 0.75	25.5 ± 1.275

3.8 Antioxidant properties

Figure 10 depicts the antioxidant activity of N1, N2, N3 nanomaterials, and Vitamin-c in the DPPH assay. They could scavenge free radicals. The percentage of inhibition increases as the concentrations of this N1, N2, N3, and Vitamin-c nanomaterials increase. At concentrations ranging from 10 to 70 g/mL, N1, N2, N3, and Vitamin-c NPs demonstrated scavenging activity, with activity percentages of 93.97%, 74.92%, 81.52%, and 94.86%, respectively, for N1, N2, N3, and Vitamin-c. In comparison to N2 and N3 NPs, N1 nanomaterials have some potential scavenging properties. The antioxidant properties of NiO nanomaterials were thought to be caused by electron transfer from the oxygen atom to the nitrogen atom in the DPPH solution, which increased inhibition of the $n \rightarrow \pi^*$ transition at 517 nm. However, based on the findings, it was determined that N1 nanomaterials have antioxidant properties and could be used in advanced clinical applications in the medical field.

Conclusions

The NiO NPs were successfully synthesized via a green process derived from various plant extracts, such as *Azadirachta indica* (N1), *Morinda citrifolia* (N2), and *Terminalia elliptica* (N3). The FESEM image of the synthesized NiO NPs confirms that are in spherical-shaped structure, and the average size of the nanoparticles is different from the N1, N2, and N3 samples. Moreover, the morphological and size analyses suggest that the NiO NPs grown from the *Morinda citrifolia* and *Terminalia elliptica* leaves than those extracted from the *Azadirachta indica* leaves due to their high surface-to-volume ratio. EDAX spectrum, the elemental percentage of the nickel in the NiO NPs was observed to be less homogeneous for the N1 sample than for the high homogeneous proportion observed for the N2 and N3 samples. This result suggests a slight compositional variation in the elemental nickel and the oxygen due to the improper development of the growth. The binding energy (BE) values decrease from left to right in the XPS spectra. These results revealed the presence of only nickel, oxygen, and carbon elements in the NiO surface matrix. The X-ray diffraction patterns show that the crystallites of the NiO NPs that were made have a center cubic structure, and the average size of the NiO is 96.95 nm. The photoluminescence study shows oxygen vacancies are higher in the N1 nanomaterials when compared to N2 and N3 NPs. The green emission at 545 and 523 nm for N1 and N2 samples. The increasing green emission band value shows an enhancement of oxygen vacancies, which is attributed to the N1 sample that can be able to produce more ROS. These ROS can damage bacterial cell components, such as nucleic acid, proteins, and macromolecules (DNA, lipids, and carbohydrates). Antibacterial activity was enhanced in N1 nanomaterials compared to N2 and N3 nanomaterials. Furthermore, from the antioxidant properties, the N1 sample demonstrates higher radical scavenging activity than the N2 and N3 samples.

Declarations

Acknowledgment

The authors would like to express our gratitude to KIRND Institute of Research and Development PVT LTD for allowing us to utilize the lab facilities, which helped in gaining expertise in various experimental techniques and conducting our study experiments.

Author Contributions:

Mr. VL carried out the preparation of the nanoparticles and executes the physical characterization studies and contributed to the main text of the manuscript. Dr. SL checked the scientific information and flow of the text to maintain a better readability. Further this research work is not funded by any agency.

Compliance with ethical standards:

Conflict of interest: The author declared that they have no conflict of interest

References

1. Porras-Alcalá, C., Moya-Utrera, F., García-Castro, M., Sánchez-Ruiz, A., López-Romero, J. M., Pino-González, M. S., ... & Sarabia, F. (2022). The Development of the Bengamides as New Antibiotics against Drug-Resistant Bacteria. Marine Drugs, 20(6), 373.
2. Saka, A., Tesfaye, J. L., Gudata, L., Shanmugam, R., Dwarampudi, L. P., Nagaprasad, N., ... & Rajeshkumar, S. (2022). Synthesis, characterization, and antibacterial activity of ZnO nanoparticles from fresh leaf extracts of Apocynaceae, Carissa spinarum L.(Hagamsa). Journal of Nanomaterials, 2022.
3. Saebnoori, E., Koupaei, N., & Hassanzadeh Tabrizi, S. A. (2022). The solution plasma synthesis, characterisation, and antibacterial activities of dispersed CuO nanoparticles. Materials Technology, 37(9), 1220-1229.
4. Preethi, T., Senthil, K., Pachamuthu, M. P., Balakrishnaraja, R., Sundaravel, B., Geetha, N., & Bellucci, S. (2022). Effect of Fe Doping on Photocatalytic Dye-Degradation and Antibacterial Activity of SnO2 Nanoparticles. Adsorption Science & Technology, 2022.
5. Qi, L., Guo, B., Lu, Q., Gong, H., Wang, M., He, J., ... & Lu, Y. (2022). Preparation and Photocatalytic and Antibacterial Activities of Micro/Nanostructured TiO2-Based Photocatalysts for Application in Orthopedic Implants. Frontiers in Materials, 9, 914905.
6. Sebastiammal, S., Bezy, N. A., Somaprabha, A., Henry, J., Biju, C. S., & Fathima, A. L. (2022). Chemical and sweet basil leaf mediated synthesis of cerium oxide (CeO2) nanoparticles: Antibacterial action toward human pathogens. Phosphorus, Sulfur, and Silicon and the Related Elements, 197(3), 237-243.
7. Karthikeyan, C., Sisubalan, N., Varaprasad, K., Aepuru, R., Yallapu, M. M., Viswanathan, M. R., & Sadiku, R. (2022). Hybrid nanoparticles from chitosan and nickel for enhanced biocidal activities. New Journal of Chemistry, 46(27), 13240-13248.
8. Aravind, M. R., Kalaiselvi, C., Revathi, B., Grace, A. N., Pitchaimuthu, S., Suresh, S., ... & Chandar, N. K. (2021). Influence of various concentrations of cetyltrimethylammonium bromide on the properties of nickel oxide nanoparticles for supercapacitor application. Nano, 16(12), 2150138.
9. Shuaib, U., Lee, D., Hussain, T., Ahmad, R., Hwang, J., Imranullah, M., ... & Shakir, I. (2022). Green synthesis of nickel oxide coupled copper hexacyanoferrate (NiO2–CuHCF) nanocomposites for

efficient and highly stable natural sunlight-driven photocatalytic degradation of wastewater pollutants. Ceramics International, 48(18), 26168-26176.

10. Husain, J., Nayak, S. M., Farheen, S., Reddy, N., Bijapur, M., Mathad, G., ... & Gurikar, S. G. (2021). Conductivity and LPG sensing behavior of polyaniline/NiO2 nano composites thin films. Ferroelectrics, 582(1), 180-186.
11. Navinprasad, A. T., Prakash, R., Yoganandh, J., Meenakshipriya, B., & Ramakrishnan, K. (2021, February). Experimental Investigation of Nickel Oxide Nanomaterials with n-Pentane Diesel Blends in Compression Ignition Engine. In IOP Conference Series: Materials Science and Engineering (Vol. 1070, No. 1, p. 012126). IOP Publishing.
12. Ma, Q., Li, H., Guo, J., Chu, S., Zhang, Q., & Lin, Z. (2021). Available surface electronic transmission of porous SnO2/NiO hollow nanofibers for the enhanced gas-sensing performance toward n-butanol. Materials Science in Semiconductor Processing, 128, 105762.
13. Ahmad, N., Ali Alghamdi, A., AL-Abdulkarim, H. A., Mustafa, G. M., Baghdadi, N., & Alharthi, F. A. (2021). Structural, morphological, and electrochemical performance of CeO2/NiO nanocomposite for supercapacitor applications. Applied Sciences, 11(1), 411.
14. Al-Shawi, S. G., Andreevna Alekhina, N., Aravindhan, S., Thangavelu, L., Elena, A., Viktorovna Kartamysheva, N., & Rafkatovna Zakieva, R. (2021). Synthesis of NiO nanoparticles and sulfur, and nitrogen co doped-graphene quantum dots/nio nanocomposites for antibacterial application. Journal of Nanostructures, 11(1), 181-188.
15. Rajakumar, G., Mao, L., Bao, T., Wen, W., Wang, S., Gomathi, T., ... & Zhang, X. (2021). Yttrium oxide nanoparticle synthesis: an overview of methods of preparation and biomedical applications. Applied Sciences, 11(5), 2172.
16. Ramya, S., Loganathan, T., Chandran, M., Priyanka, R., Kavipriya, K., Pushpalatha, G. G. L., ... & Saluja, V. (2022). Phytochemical Screening, GCMS, FTIR profile of Bioactive Natural Products in the methanolic extracts of Cuminum cyminum seeds and oil. Journal of Drug Delivery and Therapeutics, 12(2-S), 110-118.
17. Aslam, M., Abdullah, A. Z., & Rafatullah, M. (2021). Recent development in the green synthesis of titanium dioxide nanoparticles using plant-based biomolecules for environmental and antimicrobial applications. Journal of Industrial and Engineering Chemistry, 98, 1-16.
18. Humphries, R., Bobenchik, A. M., Hindler, J. A., & Schuetz, A. N. (2021). Overview of changes to the clinical and laboratory standards institute performance standards for antimicrobial susceptibility testing, M100. Journal of clinical microbiology, 59(12), e00213-21.
19. Karthikeyan, C., Sisubalan, N., Varaprasad, K., Aepuru, R., Yallapu, M. M., Viswanathan, M. R., & Sadiku, R. (2022). Hybrid nanoparticles from chitosan and nickel for enhanced biocidal activities. New Journal of Chemistry, 46(27), 13240-13248.
20. Xiong, W., Zhou, M., Huang, X., Yang, W., Zhang, D., Lv, Y., & Li, H. (2022). Direct in situ vertical growth of interlaced mesoporous NiO nanosheets on carbon felt for electrocatalytic ammonia synthesis. Chemistry–A European Journal, e202200779.

21. Zhang, H., Li, B., Zou, Y., Miao, J., Qiao, M., Tang, Y., ... & Zhu, D. (2022). Acetate promotes the formation of NiRu/NiO towards efficient hydrogen evolution. Chemical Communications, 58(61), 8556-8559.
22. Tao, S., Wen, Q., Jaegermann, W., & Kaiser, B. (2022). Formation of highly active NiO (OH) thin films from electrochemically deposited Ni (OH) 2 by a simple thermal treatment at a moderate temperature: a combined electrochemical and surface science investigation. ACS Catalysis, 12(2), 1508-1519.
23. Syahdarani, E., Ramelan, A. H., Wahyuningsih, S., Subagio, A., Kartini, I., & Kawuri, K. R. (2022, March). ZnO/NiO synthesis and its characterization using solvothermal method. In Journal of Physics: Conference Series (Vol. 2190, No. 1, p. 012015). IOP Publishing.
24. Archana, B., Sharmila, E. J., Snegapriya, M., Rangesh, K., & Susaritha, S. (2022). Fourier transform infra-red spectrochemical analyses of Pieridae butterfly wings.
25. Wu, M., Tian, L., Fu, J., Liao, S., Li, H., Gai, Z., & Gong, G. (2022). Antibacterial mechanism of Protocatechuic acid against Yersinia enterocolitica and its application in pork. Food Control, 133, 108573.

Figures

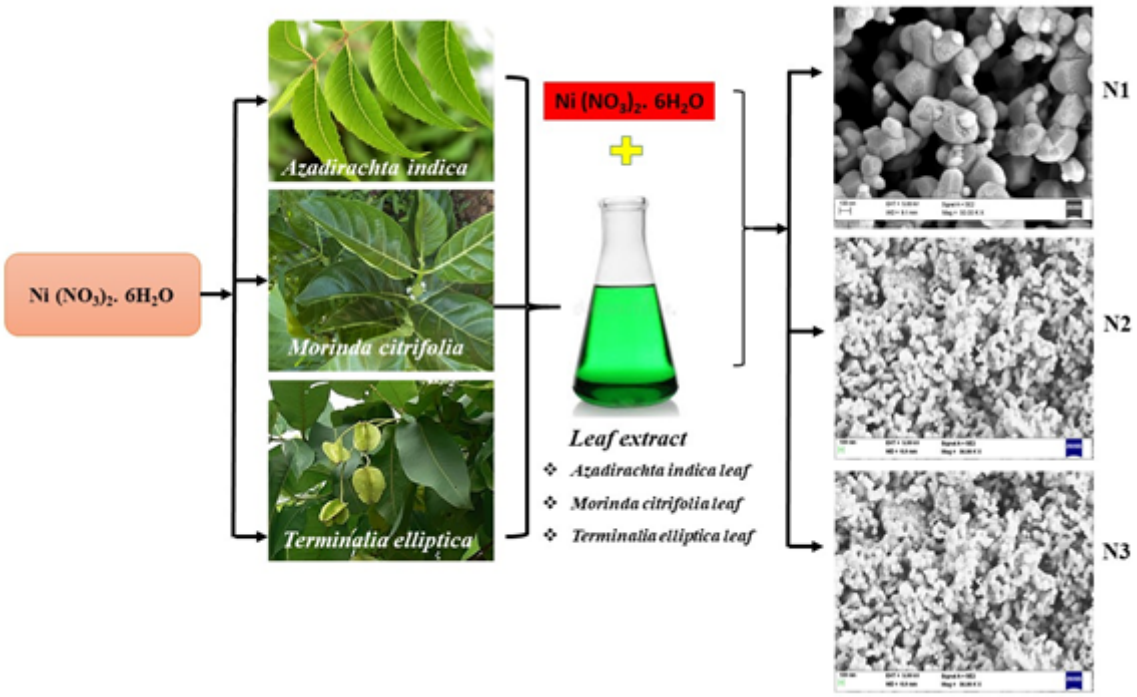

Figure 1

Schematic diagram shows the preparation of NiO NPs using different plant extract *Azadirachta indica, Morinda citrifolia*, and *Terminalia elliptica*.

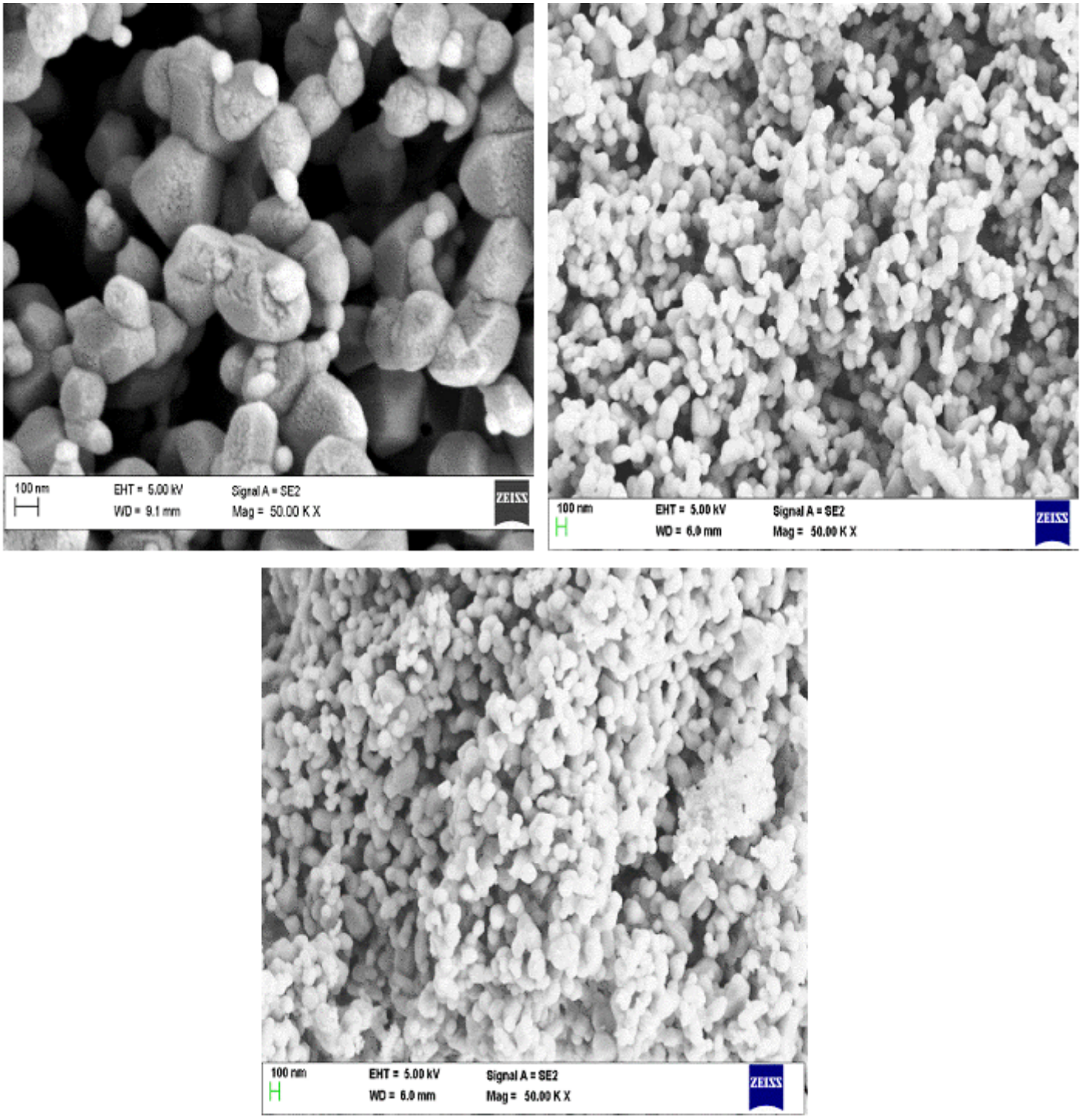

Figure 2

FESEM images NiO nanoparticles extracted from (a) *Azadirachta indica*, (b) *Morinda citrifolia* and (c) *Terminalia elliptica* leaves

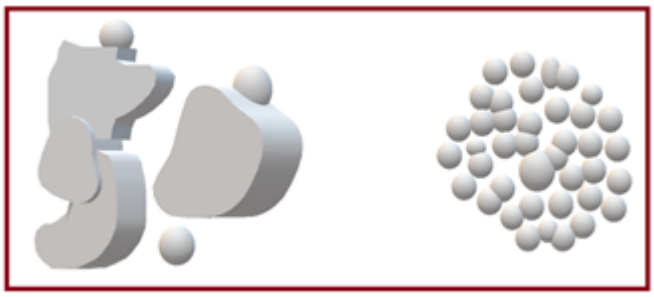

Figure 3

Schematic of the nanoparticle growth resemblance to the SEM images

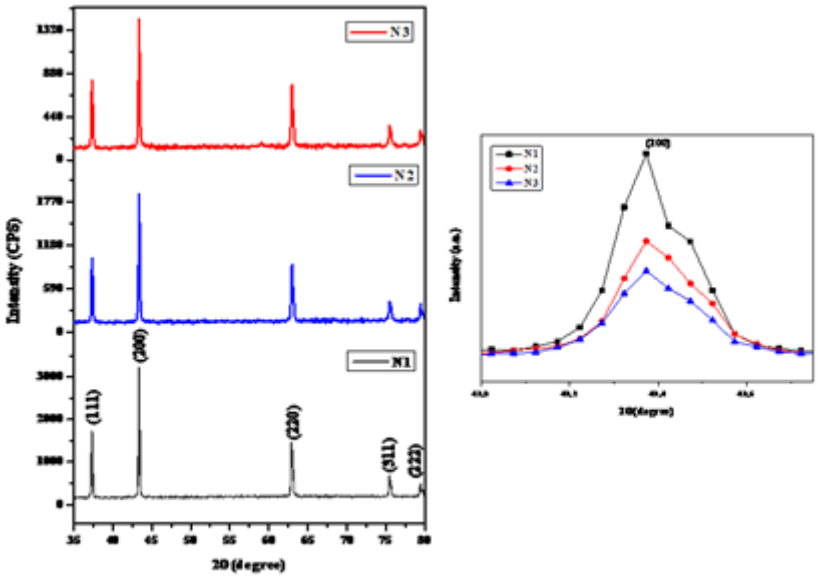

Figure 4

PXRD profiles of NiO nanoparticles extracted by green synthesis process from (a) N1, (b) N2 & (c) N3 and (d) high resolution PXRD profiles

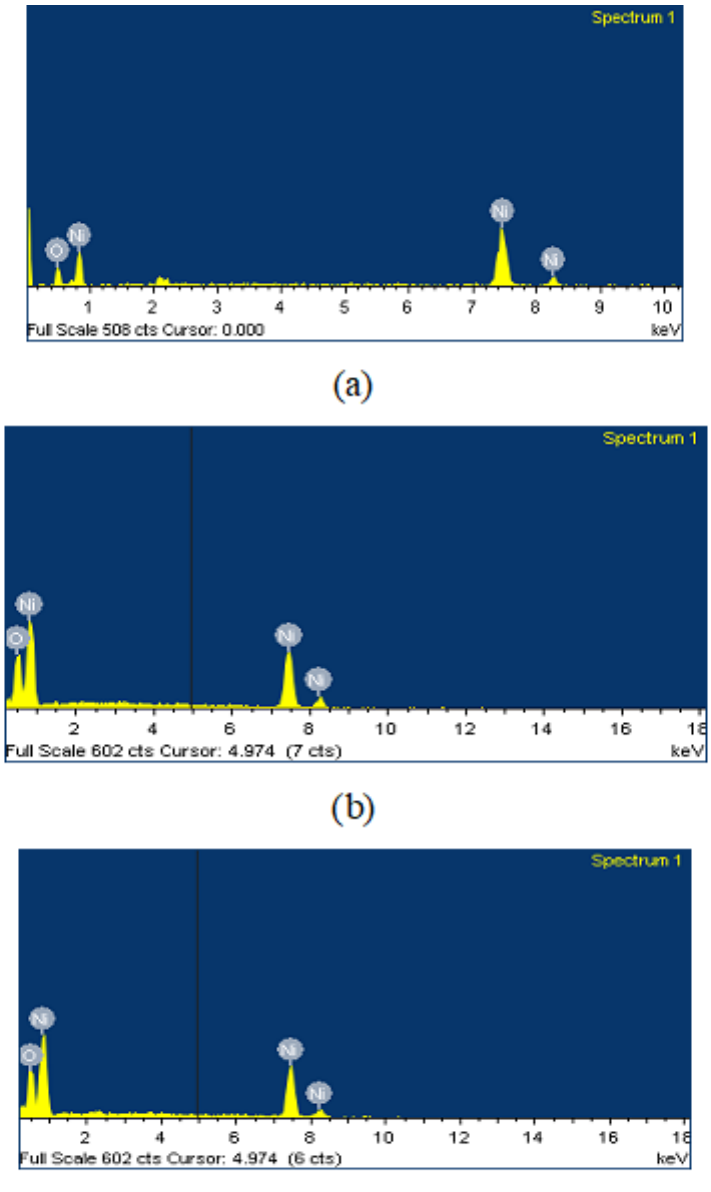

Figure 5

EDAX images of NiO nanoparticles (a) N1 (b) N2 and (c) N3 using green extraction method

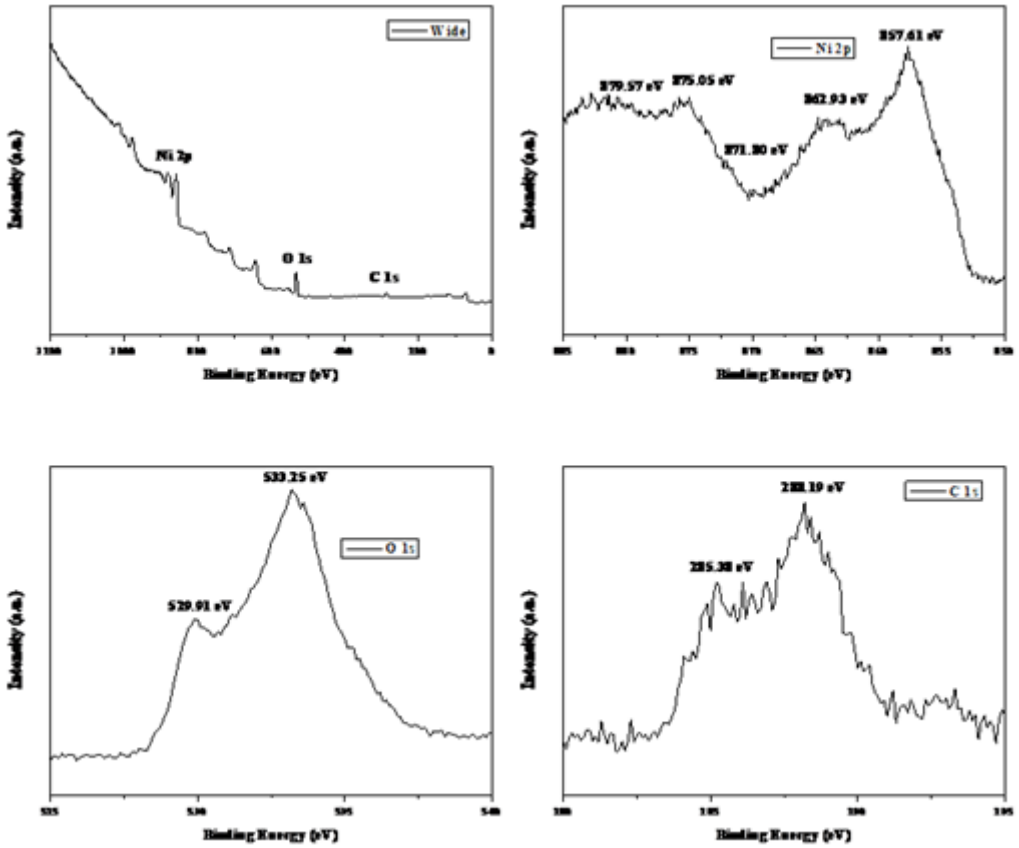

Figure 6

(a) Survey spectrum of NiO and core-level spectra of (b) C1s (c) Ni2p and (d) O1s

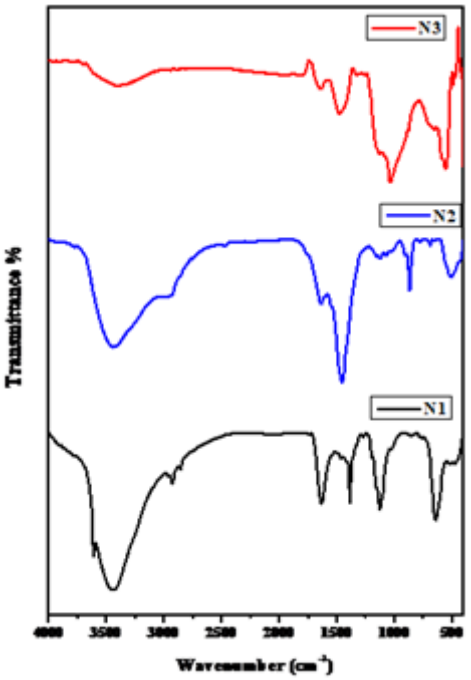

Figure 7

FTIR spectra of NiO nanoparticles extracted from the (a) N1, (b) N2 and (c) N3 leaves using green synthesis method

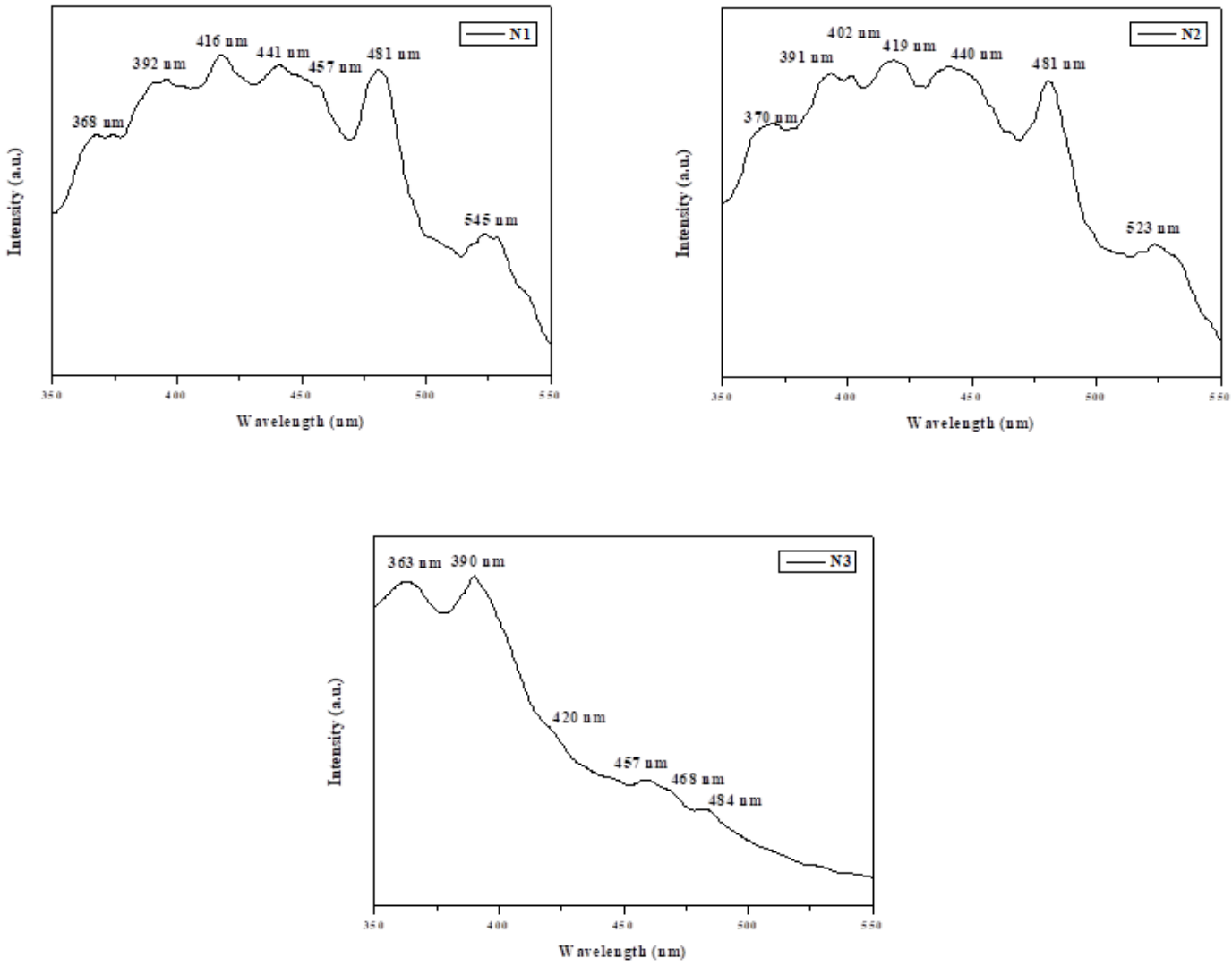

Figure 8

a. PL spectrum of NiO nanoparticles leaf extracted from *Azadirachta indica*

b. PL spectrum of NiO nanoparticles leaf extracted from *Morinda citrifolia*

c. PL spectrum of NiO nanoparticles leaf extracted from *Terminalia elliptica*

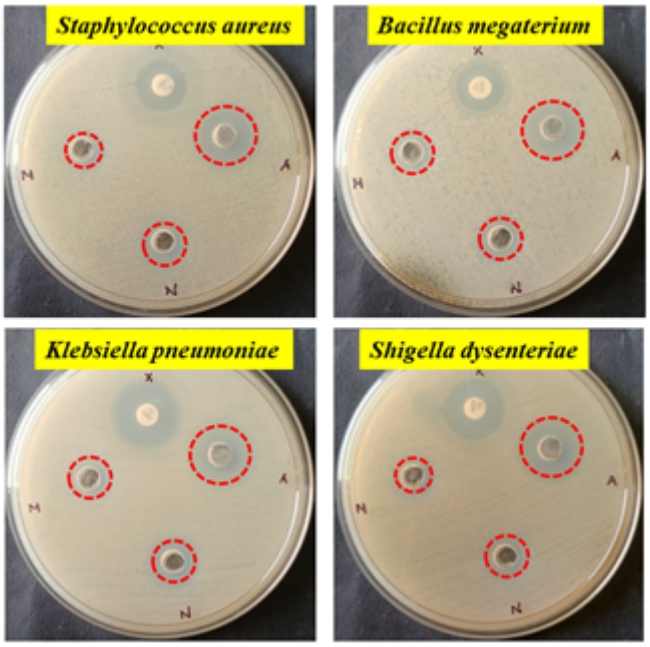

Figure 9

antibacterial activity of N1, N2 and N3 nanomaterials treated against *S. aureus, B. megaerium, K. pneumonia and S. dysenteriae* bacterias

Image not available with this version

Figure 10

This image is not available with this version.